JOURNAL OF THERMOPHYSICS AND HEAT TRANSFER
Vol. 11, No. 2, April–June 1997

Transient Natural Convection Between Vertical Finite Length Heated Plates

Kuo-Ping Chang*
Ming-Hsin Institute of Technology and Commerce, Hsinchu 30043, Taiwan, Republic of China
and
Ying-Huei Hung†
National Tsing Hua University, Hsinchu 30043, Taiwan, Republic of China

A numerical analysis of transient natural convection in vertical finite length plates with transient symmetric isoflux heating has been performed. The parameters studied are Prandtl number 0.7, channel aspect ratio 5, and steady-state Grashof numbers ranging from 10 to 10^8. From the results, it is found that the effective time when the natural convection effect becomes significant relative to conduction (τ_{on}) is strongly dependent on the steady-state Grashof number and the local position on the channel wall. In addition, transient thermal and flowfields, including isotherms, pressure contour, streamlines, and velocity profiles for various steady-state Grashof numbers are also presented and discussed. A new composite correlation of a transient-induced Reynolds number for a vertical finite length channel with various transient Rayleigh numbers is proposed. For local heat transfer characteristics along the channel surface, the transient Nusselt number at a specified location decreases with time in the beginning period of $0 \leq \tau < \tau_{on}$, whereas it gradually increases with time in the transient period of $\tau_{on} \leq \tau$. A rapid switching of heat transfer mode on transient Nusselt number distribution can be found at large steady-state Grashof numbers, say, $Gr_s > 10^5$. Finally, the present numerical steady-state results of a local Nusselt number are consistent with the existing correlation in the range of $10 \leq Gr_s \leq 10^8$.

Nomenclature

A = channel aspect ratio, L/H
Gr_s = steady-state Grashof number, $\beta g q_{cs} H^4/k\nu^2$
g = gravitational acceleration
H = channel spacing
h_x = local heat transfer coefficient
k = thermal conductivity of fluid
L = channel length
$L1$, $L2$, $L3$ = extended lengths of computational domain
Nu_x = local Nusselt number, $h_x x/k$
P = dimensionless pressure, Eq. (2)
Pr = Prandtl number, ν/α
p = fluid pressure
Q = dimensionless transient induced flow rate
q = heat flux of the plate
Ra_s = steady-state channel Rayleigh number, $\beta g q_{cs} H^5/k\alpha\nu L$
Re = transient-induced Reynolds number, Q/Gr_s
T = fluid temperature
t = time
U, V = dimensionless fluid velocity in X, Y directions, Eq. (2)
u, v = fluid velocities in x, y directions
X, Y = dimensionless coordinates, Eq. (2)
x, y = coordinates
α = thermal diffusivity of fluid
β = thermal expansion coefficient of fluid
$\Delta\tau$ = dimensionless time step
Θ = dimensionless temperature, Eq. (2)
ν = kinematic viscosity
ρ = fluid density
τ = dimensionless time, Eq. (2)
τ_{on} = dimensionless effective time of significant natural convection occurrence

Subscripts
c = transient convective value
cs = steady-state convective value
m, max = maximum value
min = minimum value
s = steady state
w = channel wall
x = local value of the quantity
0 = at ambient

Superscripts
0 = at the previous time step
– = average quantity

Introduction

STEADY-STATE natural convection in a vertical semi-infinite channel has been extensively studied.[1–6] Recently, an approximate numerical correlation of a local Nusselt number for steady-state laminar air ($Pr = 0.7$) natural convection between vertical parallel plates with unequal heat fluxes was proposed by Miyatake and Fujii.[7]

Generally, the following assumptions were made by earlier researchers in their computational studies.

1) The inlet temperature and velocity profiles were uniform.

2) The only mode of heat transfer from the channel is natural convection.

3) The channel length was assumed to be semi-infinite, i.e., the channel aspect ratio is large so that the boundary-layer approximations were valid.

Received Aug. 14, 1996; revision received Dec. 11, 1996; accepted for publication Dec. 12, 1996.

*Instructor, Department of Mechanical Engineering.
†Professor, Department of Power Mechanical Engineering. E-mail: yhhung@pme.nthu.edu.tw.

Most of the studies have dealt with boundary-layer flow, but the effect of the elliptic nature of the flow has not, to the authors' knowledge, been definitely established.

To remove any assumptions that needed to be made on the velocity and temperature profiles at the channel entrance, Ramanathan and Kumar[8] presented the numerical results of natural convective flows between two vertical parallel finite length plates within a large solid enclosure. Their results were in good agreement with those of the semi-infinite channel cases reported in the literature for large aspect ratios, but not for small aspect ratios. They concluded that this discrepancy was because of the neglect of thermal diffusion in the vertical direction of the channel. They also addressed that the geometric dimensions of the large solid enclosure were maintained at appropriate values such that the enclosure had no effect on the results. According to our observation, however, heat transfer in a finite length channel is influenced by the heat transfer between the fluid within the solid enclosure and the enclosure walls. Furthermore, their definition of Nusselt number based on the centerline temperature at the channel entrance, which varied under different Rayleigh numbers and aspect ratios, was not appropriate for interpreting the heat transfer characteristics of the finite length channel in free space, especially for low Rayleigh numbers and small aspect ratios. Moreover, no information related to the induced Reynolds number in such a configuration was reported in their study. In addition, Hung et al.[9] experimentally presented a generalized composite equation of steady-state Nusselt number at the center location of channel wall, which can be applied to the complete range of flow development in a vertical finite length channel with asymmetric isoflux heating conditions.

More recently, to consider the effects of vertical thermal diffusion and free space stratification, Lin et al.[10] performed a numerical study of steady-state natural convection within a vertical finite length channel in free space. The effect of heat conduction in the streamwise direction on the temperature distribution at the channel entrance was explored. From their results, the assumption of uniform ambient temperature distribution can be employed only for cases with both high Rayleigh numbers and high aspect ratios. For the velocity profile at the channel, a fully developed profile can be properly assumed for cases with both a small Rayleigh number and a small aspect ratio; on the other hand, a uniform velocity profile can be reasonably assumed for cases with both a large Rayleigh number and a large aspect ratio. Besides, the average steady-state channel Nusselt number and the dimensionless maximum temperatures occurred in the channel for the cases with a low Rayleigh number and these results for a small aspect ratio deviated significantly from the existing data. Finally, a new correlation of the steady-state-induced Reynolds number for a vertical finite length channel with an isoflux heating was also presented in their study.

As for the transient heat transfer behavior of natural convection, a series of investigations for transient characteristics from a vertical heated surface had been surveyed by Gebhart et al.[11] However, most calculations discussed by Gebhart et al.[11] were based on idealized postulates concerning the transient behavior of either the surface temperature or the heat flux. Specified changes of surface temperature or surface heat flux, including steps, were assumed. These kinds of transient boundary conditions are neither found in practice nor are they usually attainable in the laboratory. For the transient heat transfer behavior of natural convection in a vertical finite length channel, a careful examination of the existing literature reveals that Hung and Perng[12] were the only ones to study the transient natural convection between vertical parallel plates. They conducted a series of systematic experiments for measuring transient natural convective heat fluxes in a one-sided heated vertical channel. The effects of H and q_{cs} on the distribution of transient convective heat flux were explored. A generalized correlation was finally proposed to present the distribution of transient convective heat flux as a function of time during the power-on transient period. This correlation was presented in the following form:

$$q_c/q_{cs} = 1 - \exp(-0.0025t) \tag{1}$$

where q_c and q_{cs} represent the transient convective heat fluxes at t and steady state, respectively. The correlation was valid in the ranges of H = 0.007–0.160 mm and q_{cs} = 40–270 W/m^2 (or $\overline{Ra}_s = 2.86 \times 10^2$–$4.09 \times 10^8$).

From the foregoing literature survey, steady-state natural convection heat transfer in a vertical semi-infinite channel had been investigated theoretically and experimentally. Investigations on natural convection within a vertical finite length channel in free space were scarce, however, especially on transient heat transfer behaviors. To obtain further understanding on transient phenomena within a vertical finite length channel in free space, the present objectives are as follows:

1) Investigate the effective time of significant natural convection occurrence within a vertical finite length channel.

2) Present a new correlation of τ_{on} related to transient Grashof number and the location of interest on the channel plate.

3) Explore all relevant transient behaviors such as the transient local temperature distributions, transient maximum dimensionless temperature on channel surface, and transient local Nusselt number.

4) Propose a new composite correlation of transient-induced Reynolds number in terms of transient Rayleigh number.

Mathematical Formulation

The schematic of a vertical finite length channel considered in the present study is shown in Fig. 1. A two-dimensional, transient, laminar natural convection is induced by the buoyancy force in the fluid. Fluid properties except density are assumed constant. The density variations in the equations for the changing rate of mass and momentum are considered in the present analysis. Besides, the viscous dissipation and the compressibility effect in the energy equation are neglected.

In the present study, the primary interests are in both transient- and steady-state results on the onset of natural convection and transient characteristics under different Grashof numbers. For calculating transient natural convection solutions, a small time step of $\Delta\tau = 10^{-5}$ is chosen. In the analysis it is necessary to obtain converged results of the system of algebraic equations at each time step. Therefore, at each time step, the coefficients of the system are calculated until the converged results are obtained. At successive time steps, the results approach the steady-state values. When $t = 0$, the channel plates

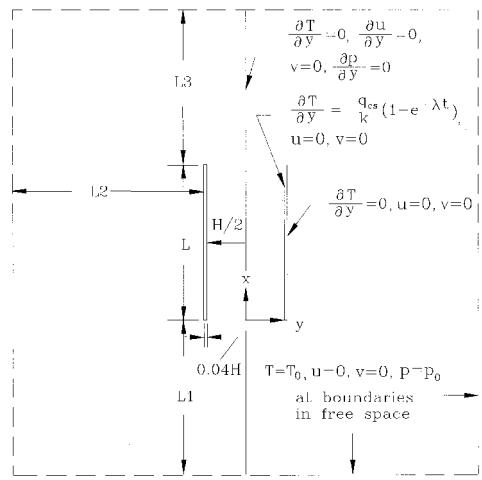

Fig. 1 Computational domain with relevant boundary conditions.

and the fluid are initially kept at the ambient temperature T_0. When $t > 0$, the channel plates are heated with a generalized correlation of transient convective heat flux expressed in Eq. (1), which was experimentally proposed by Hung and Perng.[12] The transient convective heat flux on channel plate continuously increases with time. Finally, the transient heat flux will approach a steady-state isoflux heating.

Governing Equations

With the previously mentioned assumptions and the following transformations:

$$X = \frac{x}{H} \quad Y = \frac{y}{H} \quad \tau = \frac{t\nu}{H^2} \quad U = \frac{uH}{\nu} \quad V = \frac{vH}{\nu}$$

$$P = \frac{(p - p_0)H^2}{\rho\nu^2} \quad \beta = -\frac{1}{\rho}\left(\frac{\rho - \rho_0}{T - T_0}\right) \quad A = \frac{L}{H} \tag{2}$$

$$Gr_s = \frac{\beta g q_{cs} H^4}{k\nu^2} \quad \Theta = \frac{T - T_0}{q_{cs}H/k} \quad Ra_s = \frac{\beta g q_{cs} H^5}{k\alpha\nu L} = \frac{Gr_s Pr}{A}$$

The governing equations can be written in dimensionless forms and expressed as follows:

Continuity equation:

$$\frac{1}{\rho}\left(\frac{\partial\rho}{\partial\tau} + U\frac{\partial\rho}{\partial X} + V\frac{\partial\rho}{\partial Y}\right) + \frac{\partial U}{\partial X} + \frac{\partial V}{\partial Y} = 0 \tag{3}$$

X-momentum equation:

$$\frac{\partial U}{\partial\tau} + U\frac{\partial U}{\partial X} + V\frac{\partial U}{\partial Y} = -\frac{\partial P}{\partial X} + Gr_s\Theta + \frac{\partial^2 U}{\partial X^2} + \frac{\partial^2 U}{\partial Y^2} \tag{4}$$

Y-momentum equation:

$$\frac{\partial V}{\partial\tau} + U\frac{\partial V}{\partial X} + V\frac{\partial V}{\partial Y} = -\frac{\partial P}{\partial Y} + \frac{\partial^2 V}{\partial X^2} + \frac{\partial^2 V}{\partial Y^2} \tag{5}$$

Energy equation:

$$\frac{\partial\Theta}{\partial\tau} + U\frac{\partial\Theta}{\partial X} + V\frac{\partial\Theta}{\partial Y} = \frac{1}{Pr}\left(\frac{\partial^2\Theta}{\partial X^2} + \frac{\partial^2\Theta}{\partial Y^2}\right) \tag{6}$$

Treatment of Initial and Boundary Conditions

Governing equations, Eqs. (3–6), are elliptic forms with transient term. Therefore, it is necessary to have initial and boundary conditions specified over all of the domain studied. Since the present analysis domain is symmetric, only half of the configuration is needed to simulate the problem. Moreover, since the channel-plate thickness is assumed much smaller than the channel spacing, say $H/25$, the conduction heat transfer within the plate itself can be neglected. Thus, the dimensionless initial and boundary conditions over all boundaries of the domain can be expressed as shown in the following text.

Initial Conditions

In the whole computational domain ($\tau = 0$):

$$U = V = P = \Theta = 0 \quad \text{at} \quad -L_1/H \le X \le A + L_3/H \quad \text{or} \quad 0 \le Y \le 0.54 + L_2/H \tag{7}$$

On the channel plates ($\tau = 0$):

$$\frac{\partial\Theta}{\partial Y} = 0 \quad \text{at} \quad 0 < X < A \quad Y = 0.5$$

$$\frac{\partial\Theta}{\partial Y} = 0 \quad \text{at} \quad 0 < X < A \quad Y = 0.54 \tag{8}$$

Boundary Conditions

All of the boundary conditions on the centerline symmetric boundaries, the solid-plate boundaries and extended boundaries in free space for analysis, are shown in Fig. 1. Consequently, the dimensionless boundary conditions can then be expressed in the following.

On the centerline of channel:

$$\frac{\partial U}{\partial Y} = V = \frac{\partial P}{\partial Y} = \frac{\partial\Theta}{\partial Y} = 0 \quad \text{at} \quad Y = 0 \tag{9}$$

On the channel plates:

$$U = V = 0 \quad \frac{\partial\Theta}{\partial Y} = 1 - \exp(-\lambda\tau) \quad \text{at} \quad 0 < X < A, \; Y = 0.5 \tag{10}$$

where $\lambda = 0.0025H^2/\nu$.

$$U = V = 0 \quad \frac{\partial\Theta}{\partial Y} = 0 \quad \text{at} \quad 0 < X < A, \; Y = 0.54$$

Boundary conditions in free space:

$$U = V = P = \Theta = 0 \quad \text{at} \quad X \to \pm\infty, \; Y \to \infty \tag{11}$$

For selecting a reasonable computational domain of $-L_1/H \le X \le A + L_3/H$ and $0 \le Y \le 0.54 + L_2/H$ in numerical calculations, the boundary conditions of Eq. (11) become

$$U = V = P = \Theta = 0 \quad \text{at} \quad X = -L_1/H, \; X = A + L_3/H \quad \text{or} \quad Y = 0.54 + L_2/H \tag{12}$$

For the problem under consideration, flowfields, temperature distributions, and heat transfer characteristics are usually of interest. Thus, the transient local Nusselt number representing transient local heat transfer performance in the channel is defined as

$$Nu_x = \frac{h_x x}{k} = A\left(\frac{x}{L}\right)\left[\frac{1 - \exp(-\lambda\tau)}{\Theta_w}\right] \tag{13}$$

In addition, the transient-induced flow rate in the channel can also be defined as

$$Q_c = \frac{1}{\nu}\int_0^H u \, dy = \int_0^1 U \, dY \tag{14}$$

Numerical Method

In the present research, the governing equations, Eqs. (3–6), with the associated initial conditions and boundary conditions, Eqs. (7–12), are solved numerically by the finite difference method. A staggered grid system is employed in the present study. The velocity components are calculated for the points that lie on the faces of the control volumes. Furthermore, to convert the governing equations, Eqs. (3–6), into algebraic equations known as discretization equations, the governing equations are integrated over each control volume. Thus, a set of discretization equations are derived by integrating Eqs. (3–6) over the control volume with the power-law scheme. These equations, then, are solved by using the iterative numerical scheme based on the SIMPLEC algorithm,[13] which was originally proposed by Van Doomaal and Raithby.[14]

The algebraic system of the finite difference equations is solved by the alternating direction implicit (ADI) method. At each time step, the algebraic equations are solved repeatedly with the ADI method, and the convergence criteria including

the balances of U, V, P, and T, and the overall mass for the whole computational domain are

$$\left|\frac{\phi - \phi^0}{\phi_{\max}}\right| \leq 5 \times 10^{-4} \tag{15}$$

$$\sum |Sm_p^*| \leq 10^{-3} \tag{16}$$

where ϕ represents U, V, P, or T; the superscript 0 represents the values of the variables at the previous time step; the subscript max represents the maximum value over the entire domain; and $\Sigma |Sm_p^*|$ represents the summation of absolute values of residual mass over the entire domain.

It should be noted that the Boussinesq approximation in natural convection can be employed in the present study when the steady-state Grashof number is small (e.g., $Gr_s \leq 10^6$). However, for the cases with higher steady-state Grashof numbers, say, $Gr_s > 10^6$, the grid cells in the flow region near the upper parts of the channel plates have larger absolute values of mass residual, and then the summation of absolute values of residual mass over the entire computational domain cannot be converged down to 10^{-3}. The main reason may be that the temperatures in those grid cells varied sharply because of the strong driving buoyant force, so that the Boussinesq approximation cannot be employed in all of the calculation domain. Therefore, the density-variation effect should be included in the continuity equation in the present calculations [see Eq. (3)], especially for the cases with a steady-state Grashof number higher than 10^6.

Results and Discussion

A numerical analysis of transient natural convection within a vertical finite length channel in free space has been performed in the present study. The parameters studied are Pr = 0.7, A = 5, and Gr_s ranging from 10 to 10^8. Under different Grashof numbers, the relevant transient thermal and fluid-flow characteristics such as isotherms, pressure contours, streamlines, velocity fields, local temperature distribution, maximum wall temperature distribution, buoyancy-induced flow rate, and local Nusselt number distribution are explored.

To achieve an acceptable transient numerical accuracy as well as to save computational CPU time, it is necessary to perform computational domain, grid size, and time step tests. In selecting a reasonable finite computational domain to represent an infinite free space for numerical analysis, five kinds of extended boundaries defined in Fig. 1 have been tested for steady-state cases in the study of Lin et al.[10] For a comparison of their steady-state results, the computational domain of $L_1 = L_2 = 20L$, and $L_3 = 25L$ was chosen for providing numerical results of high accuracy. Thus, the same computational domain is used in the present transient study. As for grid size test, five grid sizes, 46 (in the X direction) $\times$ 48 (in the Y direction), 70 $\times$ 72, 82 $\times$ 84, 94 $\times$ 96, and 106 $\times$ 108, are tested for the previously mentioned computational domain of $L_1 = L_2 = 20L$, and $L_3 = 25L$ with $Gr_s = 2.86 \times 10^7$, A = 3.3, and $\Delta\tau = 10^{-5}$ (Hung and Perng[12]). As compared with the transient local Nusselt number at x/L = 0.5 calculated with a grid size of 106 $\times$ 108, the average relative deviation of the results evaluated with a grid size of 94 $\times$ 96 is 0.2%, with a maximum deviation of 0.45% during the transient period of $0 < \tau < 8$. Therefore, we conclude that the grid size of 94 $\times$ 96 is acceptable and can be employed with a high numerical accuracy. Furthermore, in the present transient analysis, four time steps 1) $\Delta\tau = 4 \times 10^{-5}$, 2) 2×10^{-5}, 3) 10^{-5}, and 4) 5×10^{-6} are tested for the case of $Gr_s = 2.86 \times 10^7$ and A = 3.3 with the computational domain of $L_1 = L_2 = 20L$, and $L_3 = 25L$, and a grid size of 94 $\times$ 96. As compared with the transient local Nusselt number at x/L = 0.5 calculated with $\Delta\tau = 5 \times 10^{-6}$, the average relative deviation of the results evaluated with $\Delta\tau = 10^{-5}$ is 0.34%, with a maximum deviation of 1.45% during the transient period of $0 < \tau < 8$. Thus, we conclude that the time step of $\Delta\tau = 10^{-5}$ is acceptable for high numerical accuracy and is chosen in the present transient study.

Effective Time of Significant Natural Convection Occurrence

A transient convective heat flux dissipated from the channel surfaces with a form expressed in Eq. (1) is assumed. When τ = 0, the channel plates and the fluid are initially kept at T_0, and q_c equals zero. After the power is switched on, the channel plates are gradually heated with time. At a certain time during the transient period, the heat transfer mode within the finite length channel will switch from a pure conduction mode to a natural convection mode. Therefore, it is very interesting to explore an effective time when the natural convection effect becomes significant relative to conduction (τ_{on}) in such a geometric configuration. The effective time τ_{on} is defined as the time when the local dimensionless wall temperature Θ_H has a significant deviation, say, 5%, from that of a pure conduction mode.

From the present study, it is obvious that τ_{on} is strongly dependent on the transient Grashof number and the local position on the channel wall. At a specified location on the channel wall, τ_{on} decreases with increasing Grashof number, whereas τ_{on} increases along the streamwise direction, x/L. A similar trend for transient natural convection from a vertical heated surface had been reported by Gebhart et al.[11] By using a least-standard deviation method,[15] a new empirical correlation for predicting τ_{on} related to the steady-state Grashof number and the local position of the channel wall is proposed as follows:

$$\tau_{on} = 4.667[(x/L)/Gr_s]^{0.278} \tag{17}$$

Equation (17) is valid for the cases with Pr = 0.7, A = 5, and $Gr_s = 10^3$–10^8. As compared with the numerical transient results, the average relative deviation of the data predicted by Eq. (17) is 4.60%, with a maximum deviation of 7.25%.

Transient Thermal and Flowfields

Transient thermal and flowfields, including isotherms, pressure contour, streamlines, and velocity profiles, for the typical case of Pr = 0.7, A = 5, and $Gr = 10^5$, during the transient power-on period of $0 < \tau < 8$, are shown in Fig. 2. In this figure, the dimensionless temperature is defined as

$$\Theta_n = \Theta/\Theta_{\max} \tag{18}$$

where $\Theta_{\max}$ is the transient maximum dimensionless temperature on the plates at τ.

The dimensionless pressure is defined as

$$P_n = \frac{P - P_{\min}}{P_{\max} - P_{\min}} \tag{19}$$

where $P_{\max}$ and $P_{\min}$ are, respectively, the transient maximum and minimum pressures in the computational domain at τ. Besides, the transient velocity profile is normalized by $U_{\max}$, the transient maximum dimensionless velocity in the computational domain at τ.

It should be noted that the results for τ = 8 may be considered as steady-state data in the present study. The main reason is that the real times of τ = 8 for the cases of H = 0.08 and 0.10 m are approximated as 54.2 and 84.8 min, respectively. Thus, the consideration of τ = 8 to achieve steady-state condition is consistent with that presented by Hung and Perng.[12] They reported that the steady-state conditions were achieved within about 50 min after the power was switched on for natural convection of air within a vertical finite length channel.

From the transient isotherms shown in Fig. 2a, it is found that the temperature gradient is symmetrically developed to the channel centerline at τ = 0.05. It is also seen that the

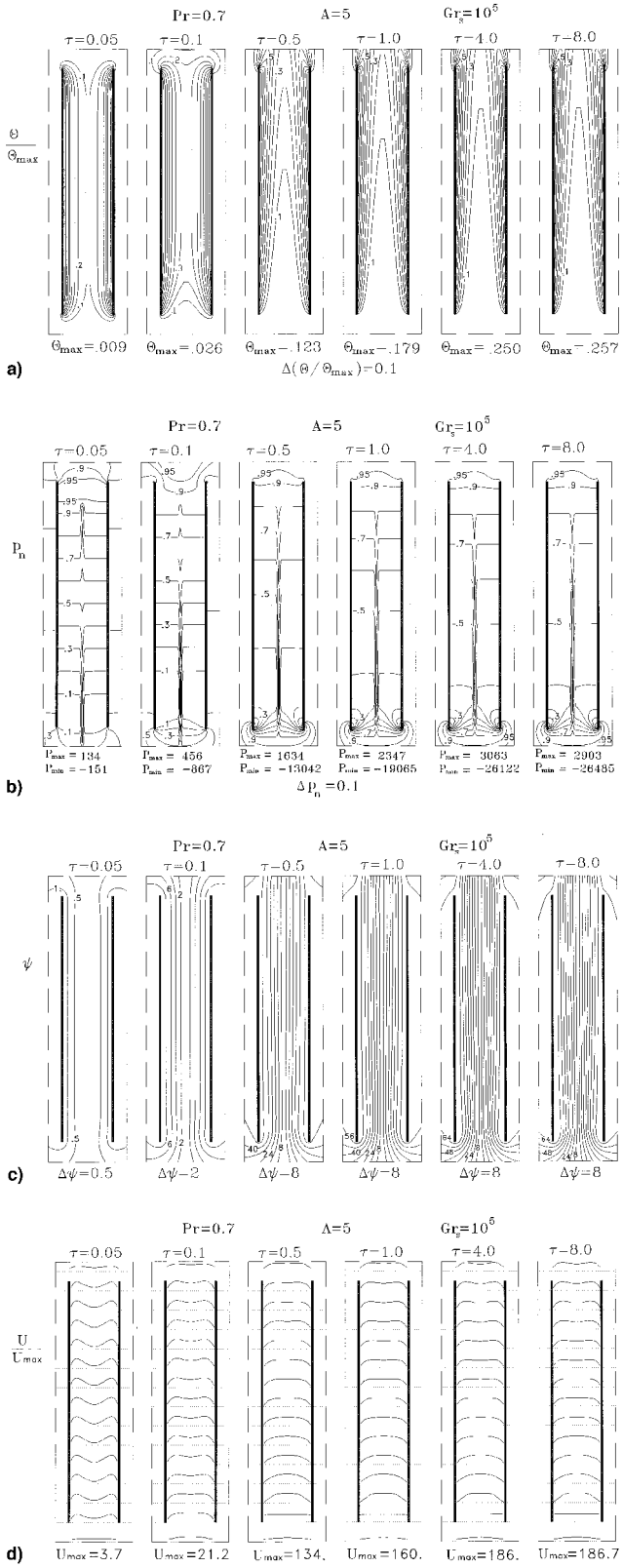

Fig. 2 Transient thermal and flowfields for Pr = 0.7, A = 5, and $Gr_s = 10^5$: a) isotherms, b) pressure contours, c) streamlines, and d) velocity profiles.

temperature distributions in the upper and lower regions of the channel are almost the same. This means the conduction mode dominates the heat transfer characteristics within the channel. When time increases to τ = 0.1, the conduction mode begins to be affected by the driving buoyancy force enhancement, and significant natural convection is about to start. After τ = 0.1, the natural convection will gradually dominate the channel heat transfer. At τ = 0.5, the effect of natural convection on transient heat transfer behaviors becomes significant. The maximum dimensionless temperature moves up to the location near the trailing edges of the channel plate (i.e., at $X = A$). When τ = 1.0, isotherms similar to those at τ = 0.5 are continuously developing. At $\tau \geq 4.0$, the steady-state condition is achieved, and the isotherms are almost identical for $4.0 \leq \tau \leq 8.0$. The relative deviation of the maximum temperatures on the channel plates for τ = 4.0 and 8.0 is 1.2%.

From the distributions of transient pressure contours shown in Fig. 2b, the high-pressure zone occurs in the region near the trailing edges of the channel plates for τ = 0.05. A very weak driving pressure gradient is induced near the inlet region of channel, and the low-pressure zone is formed near the leading edges of the channel plates. Since the driving pressure gradient is so small, the heat transfer behaviors are merely dominated by heat conduction at this time. When time increases to τ = 0.1, a significant driving pressure gradient is formed near the channel inlet region and the low-pressure zone moves up from the channel inlet. The high-pressure zone is moved away from the channel outlet. It is obvious that the induced flow is enhanced upward from the channel inlet. At $0.5 \leq \tau \leq 1.0$, the driving pressure gradient near the channel inlet region is more enhanced; and the induced flow is more developing within the channel. During the transient period of $4.0 \leq \tau \leq 8.0$, the pressure contours are almost identical. The average relative deviations of maximum and minimum pressures for τ = 4.0 and 8.0 are 1.37 and 5.51%, respectively.

As shown in Fig. 2c, the streamlines are so weak that the fluid is almost still at τ = 0.05. When time increases to τ = 0.1, the strengths of streamlines increase significantly. At $0.5 \leq \tau \leq 1.0$, the strengths of streamlines increase further. The fluid is induced into the channel not only upward from the far upstream region, but also from the lateral upstream region. The fluid flowing out from the channel looks like a jet flow. At $4.0 \leq \tau \leq 8.0$, the streamlines are almost identical.

Furthermore, the distributions of transient velocity profile are also shown in Fig. 2d. As compared with the results at τ = 8.0, the maximum velocity at τ = 0.05 is very small so that the fluid may be considered to be still within the finite length channel. When time increases to τ = 0.1, it is seen that the maximum velocity moves toward the centerline region; and the onset of the natural convection may occur. At $0.5 \leq \tau \leq 1.0$, the buoyancy force becomes stronger and the maximum velocity has moved to the centerline region to form a parabolic profile. Besides, it is also found that the velocity profile at the channel inlet is almost uniform. At $4.0 \leq \tau \leq 8.0$, the velocity profiles are almost identical. The relative deviation of maximum velocities for τ = 4.0 and 8.0 is 0.37%.

As for the effect of steady-state Grashof number on transient behaviors, the transient results, including isotherms, pressure contours, streamlines, and velocity profiles, for cases of Pr = 0.7 and A = 5 with various steady-state Grashof numbers at τ = 0.1, 1.0, and 8.0 are explored. For τ = 0.1, the temperature gradient is symmetrical in the upper and lower regions of the channel, and it is developed to the channel centerline for a low Grashof number, say, $Gr_s < 10^5$. The heat conduction is the dominating mode within the channel for lower Grashof numbers. Nevertheless, for a higher steady-state Grashof number, say, $Gr_s \geq 10^5$, it is seen that the thermal boundary layer exists throughout the channel and the natural convection dominates the channel heat transfer. The present results show that the induced pressure gradient is very weak near the inlet region of channel for $Gr_s < 10^5$; whereas, a strong pressure gradient is induced near the channel inlet region for $Gr_s \geq 10^5$. Accordingly, there are no strong streamlines occurring for $Gr_s < 10^5$, but the significant strengths of the streamlines exist in the whole channel for

$Gr_s \geq 10^5$. Additionally, the results also reveal that the fluid is induced directly upward, not only from the channel bottom region, but also from the lateral upstream region for high Grashof number cases, say, $Gr_s \geq 10^5$. The maximum velocity for $Gr_s < 10^5$ is so small, compared with that for $Gr_s \geq 10^5$, that the fluid is considered to be almost still. For high steady-state Grashof number cases, say, $Gr_s \geq 10^5$, the strong driving force generated in the region near the heated channel walls speeds the fluid up in that region of the channel. Consequently, the velocity profile with two peaks near the channel walls is generated in the channel. Similar trends for the transient thermal and fluid flow behaviors can be found for the cases of $Pr = 0.7$ and $A = 5$ with various Grashof numbers at $\tau = 1.0$ and 8.0. Note that the transient behaviors for $\tau = 1.0$ and 8.0 will be significantly affected when $Gr_s \geq 10^3$ and 10, respectively, instead of $Gr_s \geq 10^5$ for $\tau = 0.1$.

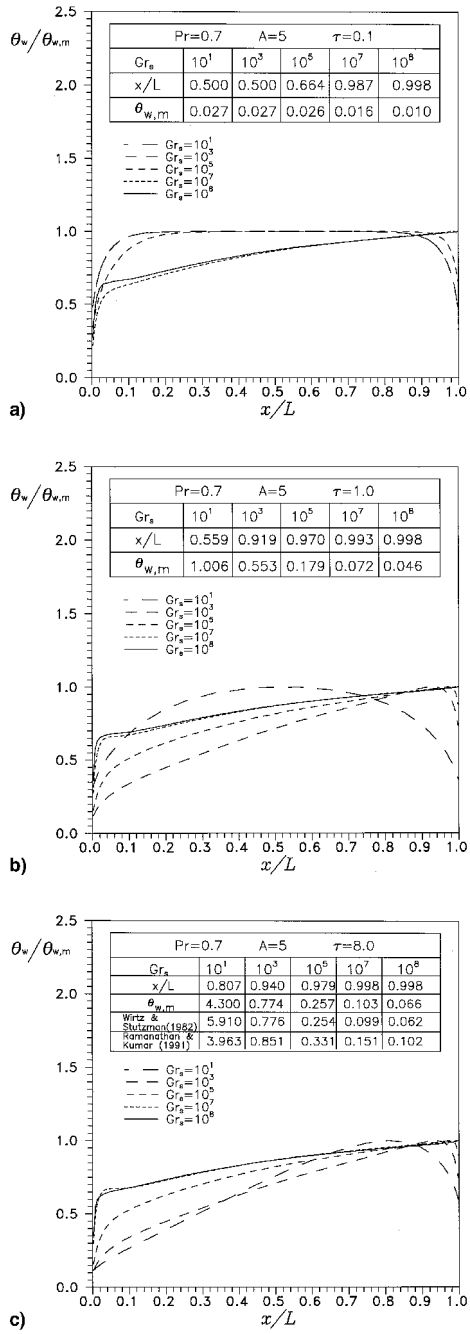

Fig. 3 Normalized transient local wall temperature distributions for cases with various steady-state Grashof numbers. τ = a) 0.1, b) 1, and c) 8.

Transient Local Temperature Distributions

For the case of $A = 5$ and $Gr_s = 10^5$, the transient local temperatures are almost uniformly distributed on the channel surface and increase with time during the period of $0.05 \leq \tau \leq 0.10$. It represents that the onset of natural convection has not yet occurred during this time period. When time increases to $\tau = 0.5$, it can be found that the local temperature near the leading edges of the channel is rapidly decreased, while that near the trailing edges is rapidly increased. The natural convection dominates the whole channel heat transfer behaviors. When $\tau = 4.0$, the maximum temperatures on the channel surface are located nearby the trailing edges of the channel plates, and the temperature profiles are almost in agreement with that at $\tau = 8.0$. The relative deviation of the maximum temperatures between $\tau = 4.0$ and 8.0 is 0.8%. Besides, the deviation of the present steady-state data, i.e., at $\tau = 8.0$, from that reported by Wirtz and Stutzman,[16] is 1.2%.

Furthermore, Fig. 3 exhibits the normalized transient local wall temperature distributions for the cases of $Pr = 0.7$ and $A = 5$ with various steady-state Grashof numbers. At $\tau = 0.1$, shown in Fig. 3a, the heat transfer characteristics in the finite length channel are mainly dominated by heat conduction for $Gr_s < 10^7$, whereas the characteristics are significantly affected by natural convection at higher steady-state Grashof numbers, i.e., $Gr_s \geq 10^7$. When time increases to $\tau = 1.0$, as shown in Fig. 3b, the heat transfer behaviors will be dominated by natural convection, except for the case of $Gr_s = 10$. When time increases further to $\tau = 8.0$, the heat transfer characteristics for all of the presently studied cases, i.e., $Gr_s \geq 10$, are dominated by natural convection.

Transient Maximum Wall Temperature Distributions

Figure 4 presents the distributions of transient maximum temperature on the channel wall. The maximum wall temperature decreases with increasing value of Gr_s at a specific transient time; and the maximum wall temperature achieves an invariant at $\tau \geq 4$. Figure 5 shows the relationship between maximum wall temperature and Grashof number at steady state. Comparisons of the present results at $\tau = 8.0$ with the existing experimental and numerical correlations of maximum steady-state wall temperature presented by Wirtz and Stutzman[16] and Ramanathan and Kumar[8] are made in Fig. 5. From these comparisons, the present results are consistent with Wirtz and Stutzman's correlation[16] at moderately large values of Gr_s, say, $Gr_s \geq 10^3$, because the maximum wall temperature occurs at the location near the trailing edge of the channel. The maximum relative deviation is less than 2.6%. Besides, a significant deviation of the present results from Ramanathan and Kumar's correlation,[8] especially for the cases at $Gr_s = 10$ and $Gr_s \geq 10^7$, can be found in Fig. 5. The reasons may be that the

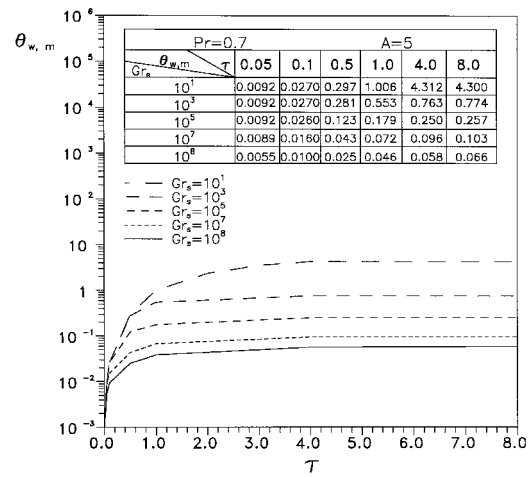

Fig. 4 Distributions of transient maximum temperature on channel wall for cases with various steady-state Grashof numbers.

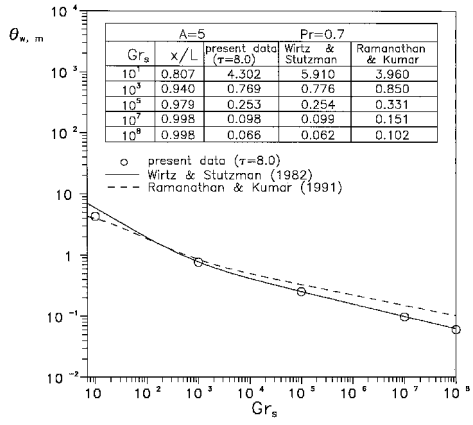

Fig. 5 Relationship between maximum wall temperature and Grashof number at steady state.

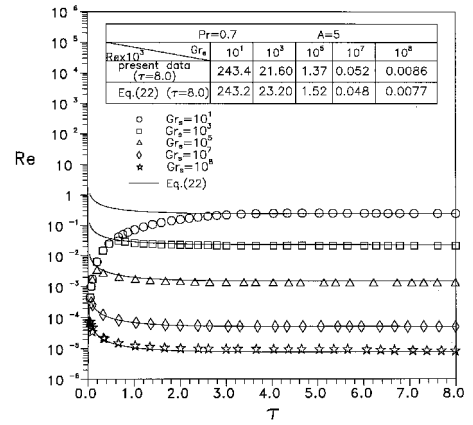

Fig. 6 Distributions of transient-induced Reynolds number for cases with various steady-state Grashof numbers.

finite length channel was confined in a solid enclosure in Ramanathan and Kumar's study.[8] The solid enclosure was not large enough so that the natural convection performance may be affected and reduced by the enclosure; consequently, larger maximum wall temperatures as compared with the present results were obtained in their numerical study.

Transient-Induced Reynolds Number

The distributions of transient-induced Reynolds number for $Pr = 0.7$ and $A = 5$ with various steady-state Grashof numbers are shown in Fig. 6. Similar to the method suggested by Churchill and Usagi,[17] which aims at obtaining an approximate composite Nu correlation by appropriately summing the Nusselt numbers of the fully developed limit and of the isolated-plate limit, a composite transient Re correlation of a vertical finite length channel with various transient Rayleigh numbers can be obtained in the following.

The derivation of the fully developed limit on the steady-state induced Reynolds number was presented by van Doormaal and Raithby.[14] Therefore, the fully developed limit of modified transient-induced Reynolds number may be expressed as

$$Re = \sqrt{\tfrac{1}{12}} Ra^{-0.5} \tag{20}$$

where the modified transient-induced channel Reynolds number is defined as $Re = Q/Gr_s$ and $Ra = (GrPr)/A$.

From the scale analysis, the order of modified steady-state-induced Reynolds number of a single plate was derived by Bejan.[18] Similarly, the modified transient-induced Reynolds number of a single plate will have the order as

$$Re \propto Ra^{-0.8} \tag{21}$$

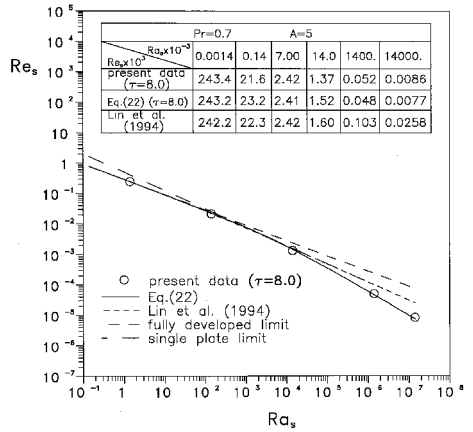

Fig. 7 Relationship between induced Reynolds number and Rayleigh number at steady state.

According to the present results, the composite transient Re correlation for a vertical finite length channel in free space can be quantitatively expressed as

$$Re = [(\sqrt{\tfrac{1}{12}} Ra^{-0.5})^{-2} + (4.02 Ra^{-0.8})^{-2}]^{-1/2} \tag{22}$$

Note that the validity of using Eq. (22) is at the transient time $\tau \geq \tau_{on}$. The average deviation of the predictions evaluated by Eq. (22) from the present numerical results is 7.52%.

Figure 7 presents the relationship between Re_s and Ra_s for the cases of $Pr = 0.7$ and $A = 5$. A steady-state correlation of a vertical finite length channel proposed by Lin et al.[10] for the cases with $Pr = 0.7$ and $1.4 \leq Ra_s \leq 3.5 \times 10^4$ is also plotted in the figure for comparison. For the cases of $Ra_s \leq 1.4 \times 10^4$, the present results at $\tau = 8.0$ are in agreement with the correlation of Lin et al.[10] However, for large Rayleigh numbers, say, $Ra_s > 1.4 \times 10^4$, a significant deviation can be found between the predictions evaluated by the correlation of Lin et al.[10] and the present results; whereas the new transient correlation presented in Eq. (22) can predict the present steady-state results well with a maximum deviation of 10.80%.

Transient Local Nusselt Number Distributions

The distributions of transient local Nusselt number for cases of $Pr = 0.7$ and $A = 5$ with various steady-state Grashof numbers at $x/L = 0.31$, 0.50, and 0.69 are shown in Figs. 8a–8c, respectively. Generally, the transient Nusselt number at a specified location decreases with time in the beginning period of $0 \leq \tau < \tau_{on}$, whereas it gradually increases with time in the period of $\tau_{on} \leq \tau \leq \tau_s$. This trend of transient Nusselt number is reasonable because the transient heat transfer behaviors are dominated by heat conduction in the beginning of the transient period and the thermal resistance will become larger as the transient boundary layer becomes thicker. When the significant natural convection occurs at τ_{on}, the heat transfer mode will switch to a significant natural convection domination from a pure heat conduction, and the transient boundary layer will become thinner gradually and approach a steady-state thickness. A rapid switching of heat transfer mode on transient Nusselt number distribution can be found at large values of Gr_s, say, $Gr_s > 10^5$.

In addition, several steady-state correlations in the existing literature are chosen to compare with the present results. From the results presented in Figs. 8a–8c, the present numerical results are consistent with the correlation reported by Hung et al.[9] in the range of $10 \leq Gr_s \leq 10^8$. The average relative deviation is 7.16%, with a maximum deviation of 10.52%. Additionally, the experimental steady-state data for the cases of $A = 3.3$ and $Gr_s = 2.8 \times 10^7$, presented by Hung and

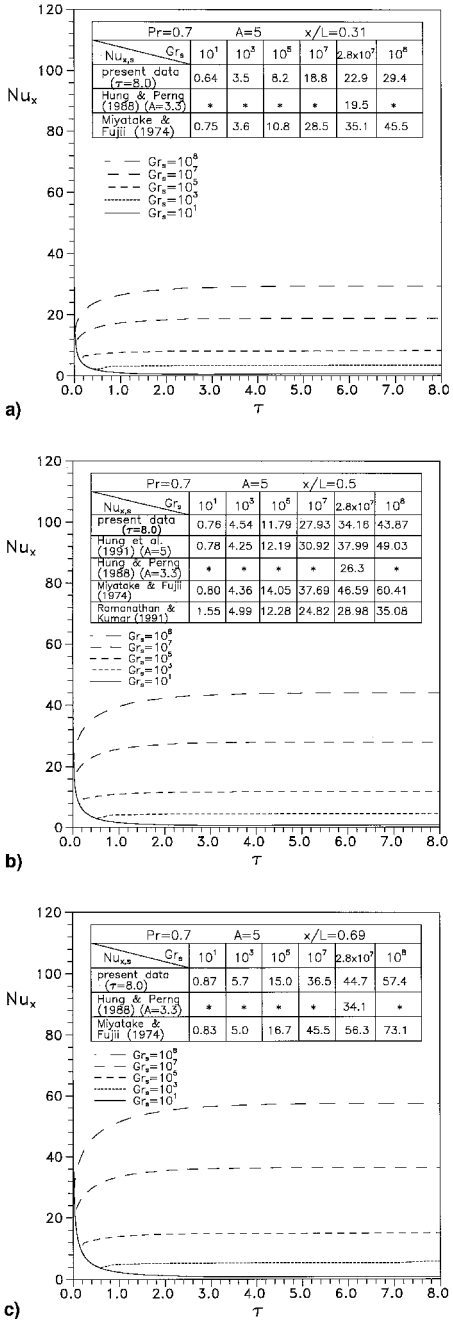

Fig. 8 Distributions of transient local Nusselt number for cases with various steady-state Grashof numbers. x/L = a) 0.31, b) 0.5, and c) 0.69.

Perng,[12] are also listed in the figures for comparison, which shows that Hung and Perng's data[12] are smaller than the present numerical results because of the effect of A. Furthermore, a good consistency between the present results and the correlation reported by Miyatake and Fujii[7] for small values of Gr_s, say, $10 \leq Gr < 10^5$, can be found. However, a significant deviation can be found for large values of Gr_s, especially for $Gr_s \geq 10^7$, because of the limitation of the Gr_s range for using Miyatake and Fujii's correlation.[7] Compared with the results reported by Ramanathan and Kumar,[8] the present results are also consistent with their correlation in the range of $10^3 \leq Gr_s \leq 10^5$. Nevertheless, a large deviation can be found for $Gr_s \geq 10^7$. The main reasons may be that the average Nusselt number in Ramanathan and Kumar's study[8] was based on the centerline temperature at the channel entry, which is different from the Nu_x based on the ambient temperature employed in the present study. Moreover, Ramanathan and Kumar's correlation cannot be applied to the cases of $Gr_s \geq 10^7$.

Conclusions

A numerical study of transient natural convection between vertical parallel finite length plates with transient symmetrical isoflux heating has been numerically conducted. The main conclusions emerging from the results and discussion may be summarized as follows:

1) The effective time when natural convection becomes significant relative to conduction is strongly dependent on the steady-state Grashof number and the local position on the channel wall. This effective time decreases with increasing steady-state Grashof number or decreasing x/L value with a power of 0.278.

2) Transient thermal and flowfields, including isotherms, pressure contour, streamlines, and velocity profiles, for the case of $Pr = 0.7$, $A = 5$, and $Gr = 10^1$–10^8 have been displayed. The transient behavior for $\tau = 1.0$ and 8.0 is significantly affected when $Gr_s \geq 10^3$ and 10, respectively, instead of $Gr_s \geq 10^5$ for $\tau = 0.1$.

3) The maximum wall temperature decreases with increasing Gr_s at a specific transient time, and the maximum wall temperature achieves an invariant at $\tau \geq 4$. Furthermore, the present results are consistent with Wirtz and Stutzman's experimental data[16] at moderately large values of Gr_s numbers, i.e., $Gr_s \geq 10^3$, because the maximum wall temperatures occurs at the location near the trailing edge of the channel.

4) At $\tau = 0.1$, the heat transfer characteristics in the finite length channel are mainly dominated by heat conduction for $Gr_s < 10^7$, whereas the characteristics are significantly affected by natural convection at higher steady-state Grashof numbers, i.e., $Gr_s \geq 10^7$. When time increases to $\tau = 1.0$, the heat transfer behavior will be dominated by natural convection, except for the case of $Gr_s = 10$. When time increases further to $\tau = 8.0$, the heat transfer characteristics for all of the present cases studied, i.e., $Gr_s \geq 10$, are dominated by natural convection.

5) A new composite correlation of transient-induced Reynolds number for a vertical finite length channel with various transient Rayleigh numbers is proposed. The correlation is valid at the transient time $\tau \geq \tau_{on}$.

6) The transient Nusselt number at a specified location decreases with time in the beginning period of $0 \leq \tau < \tau_{on}$, whereas it gradually increases with time in the period of $\tau_{on} \leq \tau \leq \tau_s$. A rapid switching of heat transfer mode on transient Nusselt number distribution can be found at large values of Gr_s, i.e., $Gr_s > 10^5$.

7) The present numerical results of a local Nusselt number are consistent with the correlation reported by Hung et al.[9] in the range of $10 \leq Gr_s \leq 10^8$.

References

[1]Elenbaas, W., "Heat Dissipation of Parallel Plates by Free Convection," *Physica*, Vol. 9, No. 1, 1942, pp. 1–28.

[2]Bodoia, J. R., and Osterle, J. F., "The Development of Free Convection Between Heated Vertical Plates," *Journal of Heat Transfer*, Vol. 84, Feb. 1962, pp. 40–44.

[3]Aung, W., "Fully Developed Laminar Free Convection Vertical Plates Heated Asymmetrically," *International Journal of Heat and Mass Transfer*, Vol. 15, No. 7, 1972, pp. 1577–1580.

[4]Aung, W., Fletcher, L. S., and Sernas, V., "Developing Free Convection Between Vertical Flat Plates with Asymmetric Heating," *International Journal of Heat and Mass Transfer*, Vol. 15, No. 7, 1972, pp. 2293–2308.

[5]Kim, S. H., Anand, N. K., and Fletcher, L. S., "Free Convection Between Series of Vertical Parallel Plates with Embedded Line Heat Sources," *Journal of Heat Transfer*, Vol. 113, Feb. 1991, pp. 108–115.

[6]Anand, N. K., Kim, S. H., and Fletcher, L. S., "The Effect of Plate Spacing on Free Convection Between Heated Parallel Plates," *Journal of Heat Transfer*, Vol. 114, May 1992, pp. 515–518.

[7]Miyatake, O., and Fujii, T., "Natural Convective Heat Transfer Between Vertical Parallel Plates with Unequal Heat Fluxes," *Heat*

Transfer—Japanese Research, Vol. 3, No. 1, 1974, pp. 29–33.

[8]Ramanathan, S., and Kumar, R., "Correlations for Natural Convection Between Heated Vertical Plates," *Journal of Heat Transfer*, Vol. 113, Feb. 1991, pp. 97–107.

[9]Hung, Y. H., Lu, C. T., and Perng, S. W., "A Composite Nu Correlation for Natural Convection in Vertical Finite-Length Channels with Asymmetric Isoflux Heating," *Proceedings of the 3rd ASME—JSME Thermal Engineering Joint Conference* (Reno, NV), American Society of Mechanical Engineers, New York, 1991, pp. 17–22.

[10]Lin, S. C., Chang, K. P., and Hung, Y. H., "Natural Convection Within a Vertical Finite-Length Channel in Free Space," *Journal of Thermophysics and Heat Transfer*, Vol. 8, No. 2, 1994, pp. 366–368.

[11]Gebhart, B., Jaluria, Y., Mahajan, R. L., and Sammakia, B., *Buoyancy-Induced Flows and Transport*, Hemisphere, New York, 1988, pp. 349–371.

[12]Hung, Y. H., and Perng, S. W., "An Experimental Technique for Measuring Transient Natural/Forced Convective Heat Fluxes in a Vertical Channel," *Experimental Thermal and Fluid Science*, Vol. 1, No. 4, 1988, pp. 305–313.

[13]Jang, D. S., Jetli, R., and Acharya, S., "Comparison of the PISO, SIMPLER and SIMPLEC Algorithms for the Treatment of the Pressure-Velocity Coupling in Steady Flow Problems," *Numerical Heat Transfer*, Vol. 10, No. 3, 1986, pp. 209–228.

[14]Van Doormaal, J. P., and Raithby, G. D., "Enhancement of the SIMPLE Method for Predicating Incompressible Fluid Flow," *Numerical Heat Transfer*, Vol. 7, No. 2, 1984, pp. 147–163.

[15]Box, E. P., Hunter, W. G., and Hunter, J. S., "Simple Modeling with Least Squares," *Statistics for Experiments*, Wiley, New York, 1978, pp. 459–509, Chap. 14.

[16]Wirtz, R. A., and Stutzman, R. J., "Experiments on Free Convection Between Vertical Plates with Symmetric Heating," *Journal of Heat Transfer*, Vol. 104, Aug. 1982, pp. 501–507.

[17]Churchill, S. W., and Usagi, R., "A General Expression for the Correlation of Rates of Transfer and Other Phenomena," *AIChE Journal*, Vol. 18, No. 6, 1972, pp. 1121–1128.

[18]Bejan, A., *Heat Transfer*, Wiley, New York, 1993, pp. 340–354.